

Stephenson, W. S.J., Naylor, L. A. , Smith, H., Chen, B. and Brayne, R. P. (2018) Wave transformation across a macrotidal shore platform under low to moderate energy conditions. *Earth Surface Processes and Landforms*, 43(1), pp. 298-311.

There may be differences between this version and the published version. You are advised to consult the publisher's version if you wish to cite from it.

Stephenson, W. S.J., Naylor, L. A. , Smith, H., Chen, B. and Brayne, R. P. (2018) Wave transformation across a macrotidal shore platform under low to moderate energy conditions. *Earth Surface Processes and Landforms*, 43(1), pp. 298-311. (doi:[10.1002/esp.4245](https://doi.org/10.1002/esp.4245)) This article may be used for non-commercial purposes in accordance with [Wiley Terms and Conditions for Self-Archiving](#).

<http://eprints.gla.ac.uk/146179/>

Deposited on: 16 February 2018

**Earth Surface
Processes and Landforms**

**Wave Transformation Across a Macrotidal Shore Platform
Under Low to Moderate Energy Conditions**

Journal:	<i>Earth Surface Processes and Landforms</i>
Manuscript ID	ESP-16-0418.R3
Wiley - Manuscript type:	Research Article
Date Submitted by the Author:	n/a
Complete List of Authors:	Stephenson, Wayne; University of Otago, Department of Geography Naylor, Larissa; University of Glasgow, School of Earth and Environmental Science; Smith, Helen; University of Exeter, College of Engineering, Mathematics and Physical Sciences Chen, Bin; Guangzhou University, School of Geography Brayne, Ralph; Centre for Environment Fisheries and Aquaculture Science, Cefas
Keywords:	Shore platform, wave energy, morphodynamics, wave transformation, infragravity

SCHOLARONE™
Manuscripts

1
2
3
4
5
6
7
8
9
10
11
12
13
14
15
16
17
18
19
20
21
22
23
24
25
26
27
28
29
30
31
32
33
34
35
36
37
38
39
40
41
42
43
44
45
46
47
48
49
50
51
52
53
54
55
56
57
58
59
60

1

2

3

4

5

6

7

8

9

10

11

12

13

14

15

16

17

18

19

20

21

22

23

24

25

26

27

28

29

30

31

32

33

34

35

36

37

38

39

40

41

42

43

44

45

46

47

48

49

50

51

52

53

54

55

56

57

58

59

60

**Wave Transformation Across a Macrotidal Shore Platform Under
Low to Moderate Energy Conditions**

Wayne S.J. Stephenson¹

Larissa A. Naylor²

Helen Smith³

Bin Chen⁴

Ralph P. Brayne⁵

¹ Department of Geography, University of Otago, PO Box 56 Dunedin, New Zealand.

² School of Geographical and Earth Sciences, College of Science and Engineering,
University of Glasgow, University Avenue, Glasgow, G12 8QQ

³ College of Engineering, Mathematics and Physical Sciences, College of Life and
Environmental Sciences, University of Exeter, Treliever Road, Penryn, Cornwall,
TR10 9EZ

⁴ School of Geographical Sciences, Guangzhou University, Guangzhou 510006,
China

⁵ Cefas, Pakefield Road, Lowestoft, NR33 0HT, UK

21

Abstract

We investigate how waves are transformed across a shore platform as this is a central question in rock coast geomorphology. We present results from deployment of three pressure transducers over four days, across a sloping, wide (~200 m) cliff-backed shore platform in a macrotidal setting, in South Wales, United Kingdom. Cross shore variations in wave heights were evident under the predominantly low to moderate (significant wave height < 1.4 m) energy conditions measured. At the outer transducer 50 m from the seaward edge of the platform (163 m from the cliff) high tide water depths were 8+ m meaning that waves crossed the shore platform without breaking. At the mid platform position water depth was 5 m. Water depth at the inner transducer (6 m from the cliff platform junction) at high tide was 1.4 m. This shallow water depth forced wave breaking, thereby limiting wave heights on the inner platform. Maximum wave height at the middle and inner transducers were 2.41 and 2.39 m respectively and significant wave height 1.35 m and 1.34 m respectively. Inner platform high tide wave heights were generally larger where energy was up to 335% greater than near the seaward edge where waves were smaller. Infragravity energy was less than 13% of the total energy spectra with energy in the swell, wind and capillary frequencies accounting for 87% of the total energy. Wave transformation is thus spatially variable and is strongly modulated by platform elevation and the tidal range. While shore platforms in microtidal environments have been shown to be highly dissipative, in this macro-tidal setting up to 90% of the offshore wave energy reached the landward cliff at high tide, so that the shore platform cliff is much more reflective.

47 Shore platform, wave energy, wave transformation, infragravity, morphodynamics

Shore platforms are a conspicuous feature of rock coasts and are also found in lakes (Allan *et al.*, 2002; Trenhaile, 2004) and estuaries (Kennedy, 2010). Many questions over the formation of shore platforms and likely future impacts of climate change remain unanswered (Naylor *et al.*, 2010; Trenhaile, 2011, 2014a). The evolution of shore platforms is complicated by variable geological settings (geology, lithology, and tectonics), long development times (> 1000 years) and sea level changes where evolution over several glacial cycles is possible (Trenhaile 2014b). Consequently the age and rates of development of shore platforms and rock coasts is difficult to resolve; although recent modelling and the application of cosmogenic dating is improving this understanding (e.g. Choi *et al.*, 2012; Thébaudeau, *et al.*, 2013; Hurst *et al.*, 2016). A holistic understanding of rock coast evolution is essential if we want to predict the resilience and vulnerability of rock coasts under changing climatic conditions.

Understanding wave transformation across shore platforms and its role in rock coast erosion is crucial to understanding the processes driving rock coast evolution. Field monitoring of wave hydrodynamics on shore platforms has been recently advanced by a number of studies investigating cross shore wave transformation and patterns of infragravity energy ($f < 0.05$ Hz) on platforms (Stephenson and Kirk, 2000; Taylor,

2003; Farrell *et al.*, 2009; Marshall and Stephenson, 2011; Ogawa *et al.*, 2011; Beetham and Kench, 2011; Ogawa *et al.*, 2012; Ogawa, 2013; Ogawa *et al.*, 2015; Ogawa *et al.*, 2016; Brayne, 2016). To date, all of these instrumented studies of wave transformation on shore platforms have occurred in micro- and mesotidal (hereafter, microtidal) environments. Ogawa (2013) reported on how wave energy is expended across a mesotidal shore platform. He reported a high degree of energy dissipation across the platform and development of infragravity energy at the inner platform. Only Trenhaile and Kanyaya (2007), Poate *et al.* 2016 and Brayne (2016) have measured waves on platforms in macrotidal settings, however these studies did not investigate energy in the infragravity frequency. Studies in microtidal settings have revealed a variety of surf zone types including highly dissipative shore platforms (Stephenson and Kirk, 2000; Ogawa *et al.*, 2012) and reflective shore platforms mixed with dissipative morphologies (Marshall and Stephenson, 2011).

A key gap in our understanding is the fate of energy delivered to rock coasts and in turn how this energy affects erosion and sediment dynamics. One approach advocated by Stephenson and Thornton (2005); Dickson *et al.* (2007) and Stephenson (2014) has been to adopt a morphodynamic framework similar to that used in beach research. In these terms rock coast morphologies can be considered reflective (e.g. plunging cliffs), intermediate (shore platforms with elements of reflection and dissipation) and dissipative (e.g. very wide platforms in shallow water). Work carried out thus far shows how tidal range, platform width, platform gradient and consequently water depth over the platform play an important role in determining the proportion of wave energy that is reflected and dissipated (Marshall and Stephenson, 2011; Beetham and Kench, 2011; Ogawa, 2013; Earlie *et al.*, 2015; Ogawa *et al.*, 2015). In microtidal environments wide platforms are highly dissipative

1
2
3
4
5
6
7
8
9
10
11
12
13
14
15
16
17
18
19
20
21
22
23
24
25
26
27
28
29
30
31
32
33
34
35
36
37
38
39
40
41
42
43
44
45
46
47
48
49
50
51
52
53
54
55
56
57
58
59
60

93 while narrow platforms are reflective at high tide. For microtidal platforms shallow
94 water depth at high tide means wave breaking dissipates significant amounts of
95 energy before reaching the landward margin of the platform where cliff retreat occurs
96 (Stephenson and Kirk, 2000). Here, waves are forced to break either before or at
97 the seaward edge of the platform. In the case of a macrotidal setting, wave energy
98 can be delivered much closer to the cliff at the back of the platform because water
99 depths are greater at high tide. It remains to be shown how much energy from
100 deepwater is expended at the cliff platform junction. In addition to examining the
101 transformation of wave energy, field investigations have shown the presence of
102 significant amounts of infragravity energy occur on dissipative microtidal platforms
103 but we are yet to demonstrate the (expected) presence of infragravity energy on
104 macrotidal platforms. Dickson *et al.* (2013) argued that infragravity energy is
105 important for the continual widening of horizontal platforms in microtidal
106 environments because infragravity energy increases water depth and allows more
107 incident wave (0.05-0.33 Hz) energy to reach the cliff foot enhancing wave erosion of
108 the cliff and aids seismic cliff shaking and weathering processes. They suggested
109 that continual widening negates the traditional model of steady state equilibrium
110 where microtidal platform widening rates decrease over time due to incident wave
111 attenuation across the widening platform. Thus, there are still important questions
112 requiring resolution about the presence and geomorphic role of infragravity energy
113 on rock coasts – especially in macrotidal settings with the least wave transformation
114 research to date.

115 We present an instrumented field study of wave transformation across a
116 macrotidal shore platform. We asked:

- 1
2
3 117 1. How are waves and energy expended across a shore platform where tidal
4
5 118 range is large (macrotidal)?
6
7 119 2. How much infragravity energy is present on a shore platform in a macrotidal
8
9 120 environment under low to moderate wave conditions?
10
11 121 3. What differences (if any) are there in wave transformation patterns between
12
13 122 this macrotidal site and the existing data on microtidal and mesotidal
14
15 123 platforms?
16
17
18
19 124

20
21
22 125 **Study Site**
23
24

25 126 The studied shore platform – cliff system is located between Nash Point and St
26
27 127 Donat's, Wales, in the semi-diurnal macrotidal Bristol Channel with a neap to spring
28
29 128 tidal range of 9 – 11 m tidal range (Figure 1) due to the resonance effects in the
30
31 129 Bristol Channel. The site is exposed to Atlantic generated storm waves exceeding
32
33 130 5.5 m, where mean annual significant wave height is approximately 2 to 2.5 m
34
35 131 (Channel Coast Observatory, 2014). Shore platforms are developed in Blue Lias
36
37 132 limestone, which is characterised by alternating thin bands of shale and thicker
38
39 133 layers of limestone (Trueman, 1930). The platforms reach widths of up to 300 m
40
41 134 although widths less than 200 m are more common. Platforms slope seaward at
42
43 135 about three degrees and follow the geological dip of the Lias (Trenhaile, 1972),
44
45 136 Platforms are backed by eroding cliffs up to 30 m high and the shore platform is
46
47 137 eroded during extreme storms (Naylor et al., 2016). The rock mass properties of the
48
49 138 Blue Lias limestone produce a platform surface which is typically comprised of wide
50
51 139 (200 – 300 m) smooth platform surfaces that are broken by near vertical steps
52
53 140 between bed layers (Stephenson and Naylor, 2011).
54
55
56
57
58
59
60

1
2
3
4
5
6
7
8
9
10
11
12
13
14
15
16
17
18
19
20
21
22
23
24
25
26
27
28
29
30
31
32
33
34
35
36
37
38
39
40
41
42
43
44
45
46
47
48
49
50
51
52
53
54
55
56
57
58
59
60

141 Wave conditions in the region can be characterised using data from the
142 Scarweather wave monitoring buoy, located approximately 40km WNW of the study
143 site. The geographical orientation of the estuary means that waves approach the site
144 almost exclusively from a WSW direction (Figure 2), with the distribution of
145 significant wave height (H_s) and mean zero-crossing period (T_z) for 2009 as
146 illustrated in Figure 2.

147

148 **Methods**

149 *Field measurements*

150 Wave measurements were made using three self-contained wave and tide
151 recorders (RBR-2050). The instruments were factory calibrated before deployment
152 and operate with a <1% measurement error. The three RBR-2050s were deployed
153 along a shore normal transect where the transducers were located at the upper
154 platform (6 m from the cliff), middle platform (90 m from the cliff) and the outer
155 platform. The outer recorder was 163 m from the cliff and 50 m from the low tide
156 edge of the platform (Figure 3). We assume waves cross the platform shore normal
157 to the shore following previously published examples (e.g. Trenhaile and Kanyaya,
158 2007; Marshall and Stephenson, 2011; Ogawa et al., 2011, 2016); this assumption
159 was validated using the SWAN wave model described below and accords with our
160 observations during fieldwork . The platform profile was surveyed using a total
161 station where elevations are reported relative to Ordnance Datum (i.e. mean sea
162 level). In order to protect the pressure transducers from the potential impact of
163 mobile boulders (e.g. Naylor *et al.*, 2016), 65 mm diameter holes were cored into the
164 platform surface using a petrol powered rock corer. The resistant nature of the

1
2
3 165 limestone beds of the Blue Lias meant that the time to taken to core these holes
4
5 166 (over an hour each) prevented locating the most seaward recorder at the absolute
6
7 167 low tide level. Each pressure transducer was placed in the hole and weighed down
8
9
10 168 using lead dive weights so that the top of the transducer was flush with the platform
11
12 169 surface. The transducer sensors were thus at the level of the platform surface while
13
14 170 recording. They were programmed to record 2048 samples at a frequency of 4 Hz,
15
16 171 beginning at 10 minute intervals. This results in 8.53 minute bursts separated by
17
18 172 2.47 minutes with no sampling (Marshall and Stephenson, 2011). Wave
19
20 173 measurements on the platform were made over four days (12:00 hrs 08-04-2009 to
21
22 174 12:00 hrs 12-04-2009) capturing eight high tides during a spring tidal sequence. The
23
24 175 raw pressure record is converted to summary wave statistics for each burst using
25
26 176 software that supports the RBR-2050. The supporting software also compensates for
27
28 177 the depth decay of the pressure signal using known coefficients for different wave
29
30 178 frequencies, the depth of deployment and water depth (Gibbons *et al* 2005). Wave
31
32 179 energy was partitioned into four frequency bands: infragravity waves (< 0.05 Hz);
33
34 180 swell waves ($0.05\text{--}0.125$ Hz); wind waves ($0.125\text{--}0.33$ Hz); and capillary waves ($>$
35
36 181 0.33 Hz) following Ogawa *et al.* (2011; 2012; 2013; 2015). Changes in wave height,
37
38 182 degree of wave attenuation, and wave energy transformations on the platform were
39
40 183 assessed from summary wave statistics and power spectral analysis conducted
41
42 184 using Matlab® (Marshall and Stephenson, 2011).
43
44
45
46
47

48 Since our wave recorders did not measure direction of wave approach nor were
49
50 186 we able to deploy instruments off shore of the platform, we undertook wave
51
52 187 modelling over the deployment period using the Simulating WAVes Nearshore
53
54 188 (SWAN) model (Booij *et al.*, 1999). A coarse grid domain, with 0.01° resolution was
55
56 189 established over the area from 3 to 5.25° W and 50.25 to 51.75° N, using offshore
57
58
59
60

1
2
3
4
5
6
7
8
9
10
11
12
13
14
15
16
17
18
19
20
21
22
23
24
25
26
27
28
29
30
31
32
33
34
35
36
37
38
39
40
41
42
43
44
45
46
47
48
49
50
51
52
53
54
55
56
57
58
59
60

190 wave boundary conditions from the European Centre for Medium-range Weather
191 Forecasting (ECMWF). The offshore boundary conditions used to drive the model
192 are shown in Figure 2. Output from the coarse grid domain model produced
193 boundary conditions for a high resolution (0.002°) nested grid domain covering the
194 Bristol Channel with a boundary at 4.25° W. SWAN was run in non-stationary mode
195 to allow a higher temporal resolution and more realistic sea state evolution. Wind
196 conditions were provided by ECMWF, and tidal heights and currents for the nested
197 model taken from predictions for Swansea, 27 km west of the study site. The model
198 was run from 5-15 April 2009, producing predictions for significant wave height, H_s ,
199 mean zero-crossing wave period, T_z , and direction at 30 minute intervals. The mean
200 zero-crossing period parameter T_z was used in preference to the mean period
201 parameter T_m to align with the data available from the wave monitoring buoys
202 detailed below.. The actual model output point is located approximately 1 km
203 offshore from the platform study site (Figure 1) to avoid modelling inaccuracies
204 associated with very shallow water at low tides. The model therefore generates wave
205 statistics at the study site before, during and after our field deployment (after Naylor
206 et al., 2016). The predicted sea states are a statistical representation of each 30
207 minute period, consequently there will be a significant number of larger individual
208 waves within each period.

209 Finally we supplemented our measured and modelled wave results with data
210 from the two nearest wave monitoring sites. The first, the Minehead buoy, which is
211 maintained by the Channel Coast Observatory (CCO, 2014) and is located at 10 m
212 water depth offshore from Minehead, on the opposite side of the Bristol Chanel,
213 approximately 18 km from our study site. The second is the Scarweather buoy, part
214 of the Cefas WaveNet network of wave monitoring buoys (Cefas, 2016), located

1
2
3 215 approximately 40 km WNW of our study site at 35 m depth (Figure 1). Data from
4
5 216 both buoys are used to provide a broader environmental context for our measured
6
7 217 and modelled wave data, however, they are too close to the study site to provide
8
9 218 boundary data for the SWAN model. Data from the buoys are summarised in Figure
10
11 219 2 .
12
13

14 220 **Results**

15
16
17 221
18
19
20
21 222 *Offshore Wave Measurements* Wave data for March and April 2009 from the
22
23 223 Bristol Channel are presented in Figure 2. Data from the Scarweather buoy provide
24
25 224 a better indication of the conditions at the platform because the buoy is fully exposed
26
27 225 to the southwesterly seas which impact on the study site, whereas the Minehead
28
29 226 buoy is in a more sheltered location. However, only significant wave heights and not
30
31 227 maximum wave heights are available for Scarweather; therefore a combination of
32
33 228 both the Minehead and Scarweather buoys were used to compare against our
34
35 229 platform wave data. A comparison of scatter plots for Scarweather buoy data for
36
37 230 2009 and the platform deployment period (Figure 2) confirms that the significant
38
39 231 wave heights experienced during the deployment are in line with the typical values
40
41 232 seen across the year. However, the wave periods during the deployment period are
42
43 233 notably higher than the average. Therefore although the wave energy levels
44
45 234 experienced during the deployment can be considered typical (since energy is
46
47 235 proportional to H_s^2), the waves are more powerful than average (with wave power
48
49 236 additionally proportional to the wave period), with potential effects on breaking
50
51 237 characteristics. Overall, we can characterise the deployment period as having low to
52
53 238 moderate energy levels (with H_s in the range of 0.45 - 3.04m) relative to storm
54
55
56
57
58
59
60

1
2
3
4
5
6
7
8
9
10
11
12
13
14
15
16
17
18
19
20
21
22
23
24
25
26
27
28
29
30
31
32
33
34
35
36
37
38
39
40
41
42
43
44
45
46
47
48
49
50
51
52
53
54
55
56
57
58
59
60

239 significant wave heights that can exceed 5.6 m in the Bristol Channel (CCO, 2014).
240 Whilst it would have been desirable to measure a wider range of energy conditions,
241 limited field deployment time restricted the opportunity to capture a full range of wave
242 conditions. Consequently, our analysis is limited to eight high tides over 4 days/96
243 hours during low to moderate energy conditions, which are similar to those
244 measured in previous studies (Table 3). .

245

246 *Offshore Modelled Waves*

247

248 Figure 4 illustrates SWAN output and is compared to the seaward wave
249 recorded on the shore platform study site. Modelled wave heights ranged from 1.09
250 m just before the deployment to 0.32 m just after the study period, and are strongly
251 influenced by the tidal elevation in the region. During the transducer deployment
252 offshore wave heights decreased. Modelled wave direction was typically between
253 240 and 250 deg, i.e. from a WSW direction. This is in contrast to the wave
254 directions of approximately 250-270 degrees seen at the Scarweather buoy (Figure
255 3), illustrating the refraction that the waves are subject to as they approach the
256 platform which leads to wave fronts breaking almost parallel to the cliff at high tide.
257 The modelled wave conditions can be characterised as low energy compared with
258 those recorded at the Scarweather buoy due to energy losses from nearshore
259 interactions. In comparison to waves recorded on the outer edge of the platform,
260 modelled wave heights were smaller, likely reflecting shoaling transformation of
261 wave height as waves enter shallower water.

262

263 *Incident Waves*

264 Water level and wave heights (H_{sig} and H_{max}) over the eight tides of the
265 deployment are displayed in Figure 5. Where data gaps occur these are during low
266 tides when the instruments were exposed. Over the period of deployment H_{sig}
267 ranged from 1 to 1.43 m and H_{max} did not exceed 2.41 m (Table 4). This represents
268 non-storm conditions.

269 At all recorders, over the entire deployment interval, the mean significant wave
270 period was nine seconds but ranged from 3.2 to 13 s. This wide range of wave
271 periods results from the occurrence of both wind and swell waves during the
272 deployment, with short period wind waves dominating the early and later part of the
273 wave record as the tide floods and ebbs over the platform (Figure. 5). Swell waves
274 generally dominated the middle of the wave record over each high tide, particularly
275 on the middle and outer part of the platform. Figure 6 illustrates a representative
276 example of one burst of data (8.5 minutes) from each of the three transducers at the
277 same time; wave groups are evident and can be clearly seen at the middle and outer
278 transducers.

279

280 *Wave Transformation*

281 The cross shore pattern of wave height (H_{sig}) is illustrated in Figure 7. At the
282 peak of the high tide the largest significant (H_{sig}) waves occurred across the inner
283 platform on seven of the eight high tides. Thus wave height tends to increase across
284 the platform as waves shoal and rise prior to breaking. However there was one

1
2
3
4
5
6
7
8
9
10
11
12
13
14
15
16
17
18
19
20
21
22
23
24
25
26
27
28
29
30
31
32
33
34
35
36
37
38
39
40
41
42
43
44
45
46
47
48
49
50
51
52
53
54
55
56
57
58
59
60

285 exception to this pattern, on 9 April, when a single H_{\max} wave recorded at the middle
286 transducer was measured at 2.41 m, 2 cm larger than the 2.39 m H_{\max} wave recoded
287 at the inner platform position in a synchronous burst. On two of the high tides waves
288 were of a similar height at all three recorders. Notably at high tide there was not a
289 pattern of decreasing wave heights across the platform; this is the opposite of what
290 is commonly found on microtidal shore platforms (Marshall and Stephenson 2011;
291 Ogawa et al. 2016). This has important implications for the capacity of waves to
292 initiate rocky shore erosion (see discussion below). These data also show a strong
293 link between shore platform elevation and wave breaking, as breaking occurs during
294 high tide at the highest platform elevation in the cross shore gradient (Figure 3). The
295 same observation was made by Brayne (2016). Figure 8 illustrates wave energy on
296 the upper platform compared to the wave energy at the middle and outer recorders
297 over the instrument deployment. There is a general pattern of higher energy on the
298 inner platform: wave energy is 300% and 335% greater compared with the outer
299 platform and the middle platform, respectively.

300 A representative sample of power spectral density (PSD) plots are presented in
301 Figure 9. In this figure synchronous 8.53 minute bursts are plotted from three days
302 for two high tides and one mid tide situation. The arrows on Figure 5 (outer recorder
303 panel) indicate the timing of these three bursts. Figure 9 show PSD at a high tide on
304 the 8 and 9 April 2009 and at mid tide on 10 April 2009. On 8 April the PSD plots are
305 dominated by energy in the swell and wind wave frequencies. On the middle and
306 outer platform there is a dominance of swell (74% and 79% respectively), and wind
307 waves account for 25% and 20% of the energy respectively. Infragravity energy is
308 1.3% at the middle transducer and less than 1% at the outer transducer. On the
309 upper platform the transducer recorded more infra-gravity (i.e. 12.2% to 13.4% of the

total energy) but there is still a dominance of energy in the wind and swell frequencies.

The pattern of energy spectra over the whole field campaign is illustrated in Figure 10. The dominance of swell wave frequencies (around 0.1 Hz) is notable where most energy is in the swell frequency band. Infragravity energy is noticeably absent from the outer and middle platform, except for the small “tail” (see circle on lower panel of Figure 10. as an example) as the tide rises across the platform. On the upper recorder more infragravity energy is evident at high tide. These patterns are indicative of the low energy conditions measured.

Discussion

Our results clearly show that under low to moderate energy conditions wave characteristics across this macrotidal shore platform are tidally modulated and are influenced by variations in platform elevation. This result is consistent with previous studies in microtidal (Stephenson and Kirk, 2000; Marshall and Stephenson, 2011; Ogawa *et al.*, 2011; Ogawa *et al.*, 2012), mesotidal (Ogawa, 2013) and macrotidal (Trenhaile and Kanyaya, 2007; Brayne, 2016; Poate *et al.*, 2016) settings. However the pattern of wave energy dissipation and reflection across the macrotidal platform measured here differs from that of previous studies.

Cross Platform Transformation

Under low to moderate energy conditions we found that similar sized or larger waves occurred on the inner platform at high tide compared to the middle and outer

1
2
3
4
5
6
7
8
9
10
11
12
13
14
15
16
17
18
19
20
21
22
23
24
25
26
27
28
29
30
31
32
33
34
35
36
37
38
39
40
41
42
43
44
45
46
47
48
49
50
51
52
53
54
55
56
57
58
59
60

333 platform. On the macrotidal shore platform reported here, deep water depths (~8 m)
334 at high tide allows waves to cross the platform with relatively little change in wave
335 height due to shoaling, where they break close to the cliff platform junction. The
336 exact position of the high tide breaking point will depend on the ratio of wave height
337 to water depth, which is modulated by platform elevation (Brayne, 2016). During our
338 study, high tide wave breaking was limited to within 6 m of the cliff-platform junction
339 (assuming $H/h = 0.73$). Thus the high tide surf zone is restricted to a narrow zone
340 (e.g. 5-6% of platform width for a 1 m wave) on the inner part of the platform, where
341 width of the surf zone is a function of water depth, platform elevation and wave
342 height. When waves are less than 2 m at high tide, 90% of the platform is crossed by
343 waves before breaking can occur. The surf zone occupies ~ 10% of the platform at
344 high tide where the outer edge of the shore platform is only important around low tide
345 when wave energy is focussed here. Using tidal inundation data (Figure. 5) we
346 calculated that this window is approximately 30 minutes in duration on each flood
347 and ebb tide (~ 60 minutes per tidal cycle). At high tide water depths across the
348 much of the platform are too great for moderate waves to break and consequently
349 there is little opportunity for waves to cause meso-scale platform erosion (cobble and
350 boulder sized erosion products, e.g. Naylor *et al.*, 2012) and boulder transport
351 (Naylor *et al.*, 2016). Consequently, this platform is likely to have a more reflective
352 morphology than that of dissipative platforms, since high tide wave energy is
353 expended in a relatively narrow zone on the upper part of the platform close to the
354 reflective cliff (or steep boulder beaches where these occur).

355 While we have not measured waves during storm events, it can be expected that
356 larger storm waves will create a wider surfzone, where the entire width of the surf
357 zone will enlarge over the shore platform as the tides ebb and flow. Data on

platform erosion and boulder transport from Naylor et al. (2016) confirms this, as platform erosion and boulder transport occurred across the mid and upper intertidal zone during storm conditions. There will be some dissipation across the platform but it is likely far greater amounts of wave energy will be able to reach the upper part of the platform and the landward cliff than we measured under low to moderate wave climate.

Wave Height and Water Depth

Only two previous investigations of wave breaking on shore platforms have compared the surf zone wave height and water depth ratio commonly applied to beaches. Farrell *et al.* (2009) using H_{rms} , showed that the wave breaking height on a shore platform in Portugal was 42% of the water depth, which is similar for wave breaking in the surf zone of sandy beaches (Thornton and Guza, 1982). Ogawa *et al.* (2011) demonstrated H_{max} was limited to 0.7 water depth (h) and H_{sig} was 0.4 h . This relationship generally held across the platform although there was some variability on the seaward edge. Figure 11 shows the pattern of wave height and water depth across the Glamorgan platform by plotting H_{sig} and H_{max} against water depth. On the inner platform wave height is controlled by water depth (which is in turn modulated by platform elevation) with H_{sig} approximately 0.74 h . Using Pearson's correlation, the relationship is significant at 0.000. At the middle platform $R^2 = 0.14$ and significant at 0.000. While at the outer platform $R^2 = 0.13$ and significant at 0.000. These low R^2 values are expected given that for much of the time particularly during mid to high tide, water depths are too great to force breaking. H_{max} at the upper platform $R^2 = 0.78$ and is significant at 0.000. H_{max} at the mid platform site $R^2 = 0.12$

1
2
3
4
5
6
7
8
9
10
11
12
13
14
15
16
17
18
19
20
21
22
23
24
25
26
27
28
29
30
31
32
33
34
35
36
37
38
39
40
41
42
43
44
45
46
47
48
49
50
51
52
53
54
55
56
57
58
59
60

382 and is significant at 0.000. At the outer platform the R^2 value was 0.07 and also
383 significant at 0.000. Results such as these are consistent with Trenhaile and
384 Kanyaya (2007) and the low values for the middle and outer platform are as a result
385 of water depths being far greater than wave height over the peak of the high tide.
386 Thus wave breaking is a function of water depth determined by the level of tidal
387 inundation and platform elevation which was also observed by Brayne (2016) on
388 macrotidal shore platforms. Similar to Ogawa *et al.* (2011) there is a degree of
389 scatter around the best fit line for the inner platform wave recording site. We
390 attribute this to the variable water depths and small wave heights.

391
392 *Infragravity Energy*

393 Our field data unsurprisingly confirms the presence of infragravity energy on a
394 macrotidal shore platform. At high tide in microtidal settings wave breaking releases
395 infragravity energy on the outer edge of platforms and is found across the platform
396 increasing shorewards (Marshall and Stephenson, 2011; Beetham and Kench, 2011;
397 Ogawa *et al.*, 2011, Ogawa *et al.*, 2012, Ogawa, 2013). On the macrotidal platform in
398 this study, high tide wave breaking was confined to the upper part of the platform;
399 here wave breaking occurs more as a function of water depth rather than
400 topography. Under higher energy conditions and a wider surf zone there would be
401 an increase in the amount of infragravity energy available across a greater width of
402 the platform. Under low-moderate energy conditions infragravity energy was
403 insignificant across the platform with less than 12 to 13% of the total energy reaching
404 the upper platform being in the infragravity band compared with 85% measured by
405 Ogawa *et al.* (2012). Taylor (2003) noted that gravity energy was “lost” to the

infragravity band on platforms on the Kaikoura Peninsula in New Zealand and so not available for geomorphic work. More recent consideration of the role of infragravity energy suggests that the energy is still able to drive geomorphic change (Dickson *et al.*, 2013). Such a low percentage of energy in the infragravity band at Glamorgan does mean more energy is in the gravity wave frequency. Regardless of the types of waves, the low to moderate energy conditions measured during this study are unlikely to have much, if any, erosive consequence. Whether infragravity energy is available for meso scale (i.e. cm – m) erosion and sediment transport requires more field investigations coupling wave, erosion and transport data under higher energy conditions. While there is still much uncertainty as to the geomorphic significance of infragravity energy on rock coast erosion (Ogawa *et al.*, 2011; Dickson *et al.*, 2013) it appears that it has little, if any role under low-moderate energy conditions in this macrotidal setting.

Some authors have speculated that infragravity energy may facilitate platform abrasion when infragravity energy acts to re-suspend abrasive sediments (Beetham and Kench, 2011; Marshall and Stephenson, 2011; Ogawa *et al.*, 2012; Ogawa, 2013). However such a scenario requires suitably sized sediment to be available. At this site loose large cobbles and fine to medium sized boulders and are the dominant sediment classes available on the platform (Naylor and Stephenson, 2010) and it is unlikely that water level changes associated with infragravity energy would be able to suspend such large sediment particles.

Comparisons to previous wave transformation research

Our findings demonstrate that wave transformation across macrotidal shore platforms has fundamental differences with those measured under similar energy

1
2
3
4
5
6
7
8
9
10
11
12
13
14
15
16
17
18
19
20
21
22
23
24
25
26
27
28
29
30
31
32
33
34
35
36
37
38
39
40
41
42
43
44
45
46
47
48
49
50
51
52
53
54
55
56
57
58
59
60

430 conditions on micro to mesotidal shore platforms (Table 3). Crucially, they show that
431 macrotidal shore platforms are reflective, with narrow energy windows within which
432 geomorphic work can take place, where wave heights are greatest at high-tide, at
433 the cliff-platform junction. This is the opposite of what happens on microtidal
434 platforms (Table 3). This finding has important implications for rock coast evolution
435 models and erosion predictions for macrotidal shore platforms and associated cliffs,
436 particularly as storminess and sea levels increase. An important consequence of
437 the macrotidal setting is that the outer margins and seaward edge of the platform
438 becomes hydrodynamically disconnected from the surf zone at mid to high tide and
439 becomes part of the subtidal offshore profile. As the ebbing tide floods the platform
440 (i.e. the surf zone moves landward) the increasing water depth over the lower to mid-
441 tidal sections means direct wave influences are reduced and wave breaking moves
442 landward. On microtidal platforms relatively shallow water depths at high tide (< 1.5
443 m) mean that the surf zone influences much more of the platform where the outer
444 platform is still exposed to wave forces and currents that are capable of eroding the
445 platform and transporting debris.

446
447 **Conclusions**

448 In this macrotidal setting, waves are transformed across the study platform
449 differently to those on platforms in microtidal settings where most previous wave
450 transformation research has taken place. Rather than a reduction in wave height
451 across the shore platform (as is the case in microtidal settings), waves remain the
452 same or increase in height from the outer seaward edge to the inner margin. This
453 pattern occurs because water depth is greater than the breaking criterion for wave

heights recorded in this study, consequently wave transformation is tidally modulated. The highest wave energies were recorded at the cliff-platform junction where ~90% of the remaining platform is effectively sub-tidal at high tide. Active wave erosion of the platform is thus most likely limited to a narrow window of opportunity as the tide floods and ebbs over the platform and only when wave heights are large enough to quarry and entrain the boulder sized erosion products (Stephenson and Naylor, 2011; Naylor *et al.*, 2016). Thus wave erosion of shore platforms is closely tethered to suitable energy windows which narrows and concentrates the time period when shore platforms and cliffs are likely to be eroded by waves. Further field data, including wave measurements coupled with high resolution boulder erosion and boulder transport monitoring data, are required to validate this assumption.

Acknowledgements

W Stephenson's field work was supported by Australian Research Council grant (DP0557205). A RGS-EPSRC Small Research Grant supported L.A. Naylor. We thank Helen Jones in the University of Exeter's cartographic unit for making Figure 1. Our special thanks to James Mendelsson for his enthusiastic support of our field work.

1
2
3 477
4
5
6 478
7
8
9 479
10
11
12 480
13
14
15 481
16
17
18 482
19
20
21 483
22
23
24 484
25
26
27 485
28
29
30 486
31

32
33 **References**
34

35
36 488
37
38
39 489 Allan JC, Stephenson WJ, Kirk, RM, Taylor A. 2002. Lacustrine shore platforms at
40
41 490 Lake Waikaremoana, North Island, New Zealand. *Earth Surface Processes*
42
43 491 *and Landforms* **27**: 207-220.
44
45
46
47 492 Beetham EP, Kench PS. 2011. Field observations of infragravity waves and their
48
49 493 behaviour on rock shore platforms. *Earth Surface Processes and Landforms*
50
51 494 **36**: 1872-1888.
52
53
54
55
56
57
58
59
60

- 495 Booij N, Ris RC, Holthuijsen LH. 1999. A third-generation wave model for coastal
496 regions 1. Model description and validation. *Journal of Geophysical Research*
497 C: Oceans, 104(4), 7649–7666.
- 498 Brayne, R.P. 2016. The Relationship between Nearshore Wave Conditions and
499 Coarse Clastic Beach Dynamics. Unpublished PhD Thesis, Exeter University.
- 500 Cefas, 2016. WaveNet, [online] available at: [https://www.cefas.co.uk/cefas-data-](https://www.cefas.co.uk/cefas-data-hub/wavenet/)
501 [hub/wavenet/](https://www.cefas.co.uk/cefas-data-hub/wavenet/) [accessed 5/9/16]
- 502 Channel Coast Observatory 2014.
503 [http://www.channelcoast.org/reports/index.php?link=&dla=download&id=550&](http://www.channelcoast.org/reports/index.php?link=&dla=download&id=550&cat=28/WaveReport2009_Mhd.pdf)
504 [cat=28/WaveReport2009_Mhd.pdf](http://www.channelcoast.org/reports/index.php?link=&dla=download&id=550&cat=28/WaveReport2009_Mhd.pdf) accessed 20-01-2014.
- 505 Choi KH, Seong YB, Jung PM, Lee SY. 2012. Using cosmogenic ^{10}Be dating to
506 unravel the antiquity of a rocky shore platform on the West Coast of Korea.
507 *Journal of Coastal Research* **28**: 641-657.
- 508 Dickson ME, Ogawa H, Kench PS, Hutchinson A. 2013. Sea-cliff retreat and shore
509 platform widening: steady-state equilibrium? *Earth Surface Processes and*
510 *Landforms* **38**: 1046-1048.
- 511 Dickson M, Walkden M, Hall J. 2007. Systemic impacts of climate change on an
512 eroding coastal region over the twenty-first century. *Climatic Change* **84**: 141-
513 166.
- 514 Earlie, CS, Young, AP, Masselink, G, Russell, PE. 2015. Coastal cliff ground motions
515 and response to extreme storm waves. *Geophysical Research Letters* **42**(3)
516 846-854. doi: 10.1002/2014GL062534

1
2
3
4
5
6
7
8
9
10
11
12
13
14
15
16
17
18
19
20
21
22
23
24
25
26
27
28
29
30
31
32
33
34
35
36
37
38
39
40
41
42
43
44
45
46
47
48
49
50
51
52
53
54
55
56
57
58
59
60

517 Farrell EJ, Granja H, Cappiotti L, Ellis JT, Li B, Sherman DJ. 2009. Wave
518 Transformation across a rock platform, Belinho, Portugal. *Journal of Coastal*
519 *Research SI 56*: 44–48.

520 Gibbons DT, Jones G, Siegel E, Hay A, Johnson F. 2005. Performance of a new
521 submersible tide-wave recorder, in Oceans, 2005. Proceedings of MTS/IEEE,
522 vol. 2, pp. 1057–1060, IEEE, New York.

523 Hurst MD, Rood DH, Ellis MA, Anderson RS, Dornbusch U. 2016. Recent
524 acceleration in coastal cliff retreat rates on the south coast of Great Britain.
525 *Proceedings of the National Academy of Sciences 113*:13336-13341.

526 Kennedy DM, 2010. Geological control on the morphology of estuarine shore
527 platforms: Middle Harbour, Sydney, Australia. *Geomorphology 114*: 71 - 77.

528 Marshall RJE, Stephenson WJ. 2011. The morphodynamics of shore platforms in a
529 microtidal setting: Interactions between waves and morphology. *Marine*
530 *Geology 288*: 18-31.

531 Naylor LA, Coombes MA, Viles HA. 2012. Reconceptualising the role of organisms in
532 the erosion of rock coasts: A new model. *Geomorphology 157-158*: 17-30.

533 Naylor LA and Stephenson WJ. 2010. On the role of discontinuities in mediating
534 shore platform erosion. *Geomorphology 114*: 89-100.

535 Naylor LA, Stephenson WJ, Trenhaile AS. 2010. Rock coast geomorphology: Recent
536 advances and future research directions. *Geomorphology 114*: 3-11.

537 Naylor LA, Stephenson WJ, Smith HC, Way O, Mendelssohn J, Cowley A. 2016.
538 Geomorphological control on boulder transport and coastal erosion before,

539 during and after an extreme extra-tropical cyclone. *Earth Surface Processes &*
540 *Landforms*. **41**: 685-700.

541 Naylor LA, Viles HA 2000. A temperate reef builder: an evaluation of the growth,
542 morphology and composition of *Sabellaria alveolata* (L.) colonies on
543 carbonate platforms in South Wales. Geological Society, London, Special
544 Publications **178**: 9-19.

545 Ogawa H. 2013. Observation of wave transformation on a sloping type B shore
546 platform under wind-wave and swell conditions. *Geo-Marine Letters* **33**: 1-11.

547 Ogawa H, Dickson ME, Kench PS. 2011. Wave transformation on a sub-horizontal
548 shore platform, Tatapouri, North Island, New Zealand. *Continental Shelf*
549 *Research* **31**: 1409-1419.

550 Ogawa, H, Dickson, ME, Kench, PS. 2015. Hydrodynamic constraints and storm
551 wave characteristics on a sub-horizontal shore platform. *Earth Surface*
552 *Processes and Landforms* **40**: 65–77.

553 Ogawa H, Dickson ME, Kench PS. 2016. Generalised observations of wave
554 characteristics on near-horizontal shore platforms: Synthesis of six case
555 studies from the North Island, New Zealand. *New Zealand Geographer* **50**:
556 107-121.

557 Ogawa H, Kench P, Dickson M. 2012. Field Measurements of Wave Characteristics
558 on a Near-Horizontal Shore Platform, Mahia Peninsula, North Island, New
559 Zealand. *Geographical Research* **50**: 179-192.

560

1
2
3
4
5
6
7
8
9
10
11
12
13
14
15
16
17
18
19
20
21
22
23
24
25
26
27
28
29
30
31
32
33
34
35
36
37
38
39
40
41
42
43
44
45
46
47
48
49
50
51
52
53
54
55
56
57
58
59
60

561 Poate TG, Masselink G, Austin MA, Dickson ME, Kench P.S 2016. Observations of
562 Wave Transformation and Macro-tidal Rocky Platforms. *Journal of Coastal*
563 *Research* SI **75**: 602-606.

564 Stephenson W. 2014. Rock coasts. In Masselink, G and Gehrels, R. (Eds.), *Coastal*
565 *environments & global change*. (pp. 356-379). Chichester, UK: Wiley.

566 Stephenson WJ, Kirk RM. 2000. Development of shore platforms on Kaikoura
567 Peninsula, South Island, New Zealand: Part One: The role of waves.
568 *Geomorphology* **32**: 21-41.

569 Stephenson WJ, Naylor LA. 2011. Geological controls on boulder production in a
570 rock coast setting: Insights from South Wales, UK. *Marine Geology* **283**: 12-
571 24.

572 Stephenson WJ, Thornton LE. 2005. Australian Rock Coasts: review and prospects.
573 *Australian Geographer* **36**: 95-115.

574 Taylor AJ. 2003. Change and processes of change on shore platforms. PhD Thesis,
575 University of Canterbury, Christchurch. 386 pp.

576 Thébaudeau B, Trenhaile AS, Edwards RJ. 2013. Modelling the development of
577 rocky shoreline profiles along the northern coast of Ireland, *Geomorphology*
578 **203**: 66-78.

579 Thornton EB, Guza RT. 1982. Energy saturation and phase speeds measured on a
580 natural beach. *Journal of Geophysical Research* **87(C12)**: 9499.

581 Trenhaile AS. 1972. Shore Platforms of Vale of Glamorgan, Wales. *Transactions of*
582 *the Institute of British Geographers* 127-144.

- 1
2
3 583 Trenhaile AS. 2002. Rock coasts, with particular emphasis on shore platforms.
4
5 584 *Geomorphology* **48**: 7-22.
6
7
8 585 Trenhaile AS 2004. Lacustrine shore platforms in southwestern Ontario, Canada.
9
10 586 *Zeitschrift für Geomorphology* **48**: 441-59.
11
12
13 587 Trenhaile AS. 2011 Predicting the response of hard and soft rock coasts to changes
14
15 588 in sea level and wave height. *Climatic Change* **109**: 599-615.
16
17
18 589 Trenhaile AS 2014a. Climate change and the impact on rocky coasts. In Kennedy
19
20 590 DA, Stephenson WJ, Naylor LA. (eds), *Rock Coast Geomorphology: A Global*
21
22 591 *Synthesis*. Memoir 40, Geological Society Books, London, 7-17.
23
24
25 592 Trenhaile AS. 2014b. Modelling the effect of Pliocene-Quaternary changes in sea
26
27 593 level on stable and tectonically active land masses. *Earth Surface Processes*
28
29 594 *and Landforms* **39**: 1221-1235.
30
31
32 595 Trenhaile AS, Kanyaya JI. 2007. The role of wave erosion on sloping and horizontal
33
34 596 shore platforms in macro- and mesotidal environments. *Journal of Coastal*
35
36 597 *Research* **23**: 298-309.
37
38
39 598 Trueman AE. 1930. The Lower Lias (Bucklandii Zone) of Nash Point, Glamorgan.
40
41
42 599 *Proceedings of the Geologists Association* **41**: 148–159.
43
44
45 600

1
2
3
4
5
6
7
8
9
10
11
12
13
14
15
16
17
18
19
20
21
22
23
24
25
26
27
28
29
30
31
32
33
34
35
36
37
38
39
40
41
42
43
44
45
46
47
48
49
50
51
52
53
54
55
56
57
58
59
60

601 LIST OF FIGURES AND TABLES

602

603 Figure 1. Location of study site and wave array across a sloping macrotidal shore

604 platform on the Glamorgan coast, Wales, UK. Note SWAN model output located 1

605 km from the low tide edge of the shore platform.

606

607 Figure 2. Wave data from Minehead and Scarweather Buoys march to April 2009.

608 Box indicates period of deployment of wave recorders on the study shore platform.

609

610 Figure 3. Cross shore profile of study platform showing location of the three wave

611 recorders used in this study where platform elevation falls between stations was as

612 follows: Inner – Middle (4.2 m), Inner – Outer (6.59 m), Middle – Outer (2.39 m).

613

614 Figure 4 Comparisons of SWAN wave height output with most seaward pressure

615 transduce deployed on shore platform.

616

617 Figure 5. Wave heights (H_{sig} and H_{max}) and water depth across the shore platform

618 over the wave recorder deployment period. Arrows indicate sample bursts shown in

619 Figure 6.

Figure 6 Example of a synchronous burst samples at 12:00 hrs 08-04-2009 showing the water surface at each transducer. Wave groups are evident at the outer (c) and middle (b) wave recorders.

623

Figure 7. Cross platform variations in H_{sig} . Note slightly higher waves in the inner part of the platform compared to the middle and outer platform on six of the eight high tides.

627

Figure 8 Comparison of wave energy across the shore platform. Wave energy on the upper platform was calculated as a percentage of wave energy of the middle and outer platform.

631

Figure 9. Power spectral density plots at a high tide on the 8 and 9 April 2009 and at mid tide on 10 April 2009. The upper transducer was not inundated so there are no data for 10 April at this time stamp. Note the increased presence of infragravity energy on the middle and inner platform.

636

Figure. 10. Summary PSD plots for complete field deployment. Note wider plots for inner recorder at infragravity frequencies and thin tails of infragravity energy at middle and outer wave recorders (example denoted by ellipses).

640

1
2
3
4
5
6
7
8
9
10
11
12
13
14
15
16
17
18
19
20
21
22
23
24
25
26
27
28
29
30
31
32
33
34
35
36
37
38
39
40
41
42
43
44
45
46
47
48
49
50
51
52
53
54
55
56
57
58
59
60

641 Figure 11. Wave heights (H_{sig} and H_{max}) plotted against water depth at each wave
642 recorder position across the platform.

643

644 Table 1 Annual H_{sig} exceedance and annual maximum H_{sig} 2007 to 2011, Minehead
645 wave recorder (CCO, 2014).

646

647 Table 2. Annual H_{sig} exceedance and annual maximum H_{sig} 2007 to 2011,
648 Scarweather wave recorder (CCO, 2014).

649

650 Table 3. Synthesis of existing wave transformation data across shore platforms (H_{sig}
651 = significant wave height; H_{max} = maximum wave height; PT = pressure transducer;
652 ADC = Acoustic Doppler current meter; ECM = Electromagnetic current meter).

653

654 Table 4. Summary wave statistics, water level and pressure transduce locations.

655

656

657

658

659

660

661

662

663

664

665 Table 1.

	Annual H_{sig} exceedance* (m)						Annual Maximum (A_{max}) = H_{sig}		
Year	0.05%	0.50%	1%	2%	5%	10%	Date	A_{max}	(m)
2007	2.36	2	1.84	1.67	1.38	1.09	2-Dec-07	21:00	2.55
2008	2.7	2.17	2.01	1.78	1.5	1.27	10-Mar-08	23:00	2.77
2009	2.13	1.81	1.65	1.5	1.23	1.02	14-Nov-09	16:30	2.53
2010	2.36	1.66	1.47	1.29	1.03	0.84	31-Mar-10	10:00	2.68
2011	2.33	1.98	1.85	1.66	1.36	1.12	15-Dec-11	4:30	2.51

666

667

668

669

670

671

672

673

674

1
2
3 675
4
5
6 676
7
8
9 677 Table 2
10
11
12
13
14
15
16
17
18
19
20
21
22
23
24
25
26
27
28
29
30
31
32
33
34
35
36
37
38
39
40
41
42
43 686
44
45
46
47 687
48
49
50 688
51
52
53 689
54
55
56 690
57
58
59
60

	Annual H _{sig} exceedance (m)						Annual Maximum (Amax) = H _{sig}		
Year	0.05%	0.50%	1%	2%	5%	10%	Date		Amax (m)
2007	5.12	4.25	3.83	3.46	2.98	2.45	11-Jan-07	11:00	5.49
2008	4.89	3.8	3.53	3.28	2.82	2.41	10-Mar-08	20:00	5.43
2009 ¹	4.72	3.8	3.53	3.16	2.82	2.32	14-Nov-09	11:30	4.89
2010 ¹	5.26	3.08	2.80	2.53	2.16	1.77	11-Nov-10	23:00	5.61
2011	4.40	3.69	3.47	3.23	2.80	2.41	15-Dec-11	03:00	4.79

¹There is a gap in the dataset from 27/11/09 – 31/3/10. Note that data from 2007 and 2010-11 are post-processed following download from the buoy and quality control procedures, and are of a higher quality than the telemetry data used for 2008 and 2009. There appears to have been a problem with the post-processing which means that only telemetry data are available for the full length of these years. The telemetry data has been processed into bins of H_{sig} for transmission, hence the repeat values in the exceedance data. The accuracy is therefore slightly lower, but the trends in the data are correct. These data are sourced from the Cefas WaveNet database (<https://www.cefas.co.uk/cefas-data-hub/wavenet/>).

Table 3.

Author	Tidal Range	Platform width	Study Duration (hours)	H _{sig} (m)	H _{max} (m)	Location	Method	Size of Array
Stephenson and Kirk, (2000)	Micro	85-88	96	0.2-0.5	1.1	NZ	PT	4
Taylor, (2003)	Micro	85	60	0.2-0.5	0.3-0.7	NZ	ADCP ECM	12
Stephenson and Thornton (2005)	Micro	30	96	0.17-0.80		Australia	PT	2
Trenhaile and Kayana, (2007)	Meso Macro	100-180	96	0.25-0.85		Canada	Video camera and Poles	10 poles
Farrell <i>et al.</i> (2009)	Meso	70	40		0.92-1.14	Portugal	PT	7
Marshall and Stephenson (2011)	Micro	58 61 66 138	2×144	0-0.74		NZ & Australia	PT	3-5
Beetham and Kench (2011)	Micro	130 270	36	< 0.8		NZ	PT	5
Ogawa (2011)	Micro	250	24	0.4 – 0.6 m	0.86	NZ	PT	4
Ogawa <i>et al.</i> (2012)	Micro	140	24	0.5 – 0.6 m		NZ	PT	5
Ogawa (2013)	Meso	81	24	0.72 – 1.18		NZ	PT	5
Poate <i>et al.</i> (2016)	Macro					UK	PT	15
THIS PAPER	Macro	~200 m.	96	1.43	2.41	Wales, UK	PT	3

1
2
3
4
5
6
7
8
9
10
11
12
13
14
15
16
17
18
19
20
21
22
23
24
25
26
27
28
29
30
31
32
33
34
35
36
37
38
39
40
41
42
43
44
45
46
47
48
49
50
51
52
53
54
55
56
57
58
59
60

698

699

700

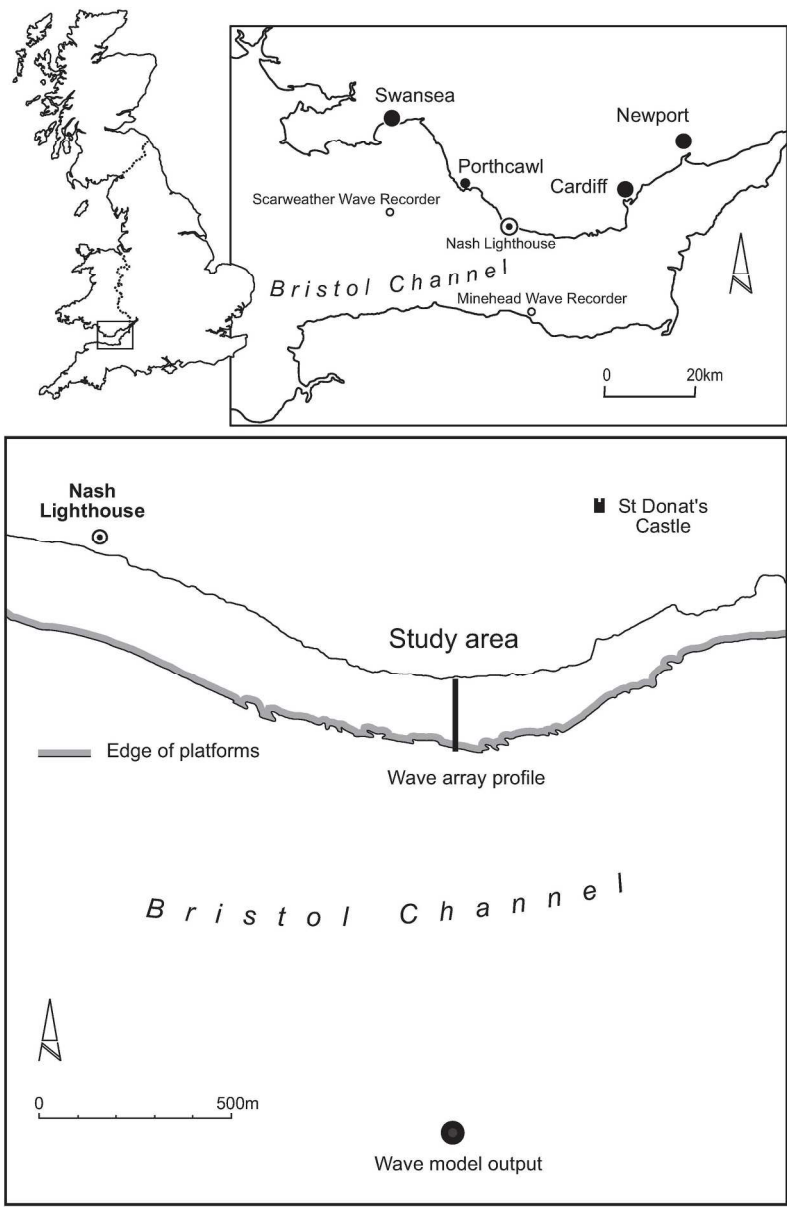
701

702

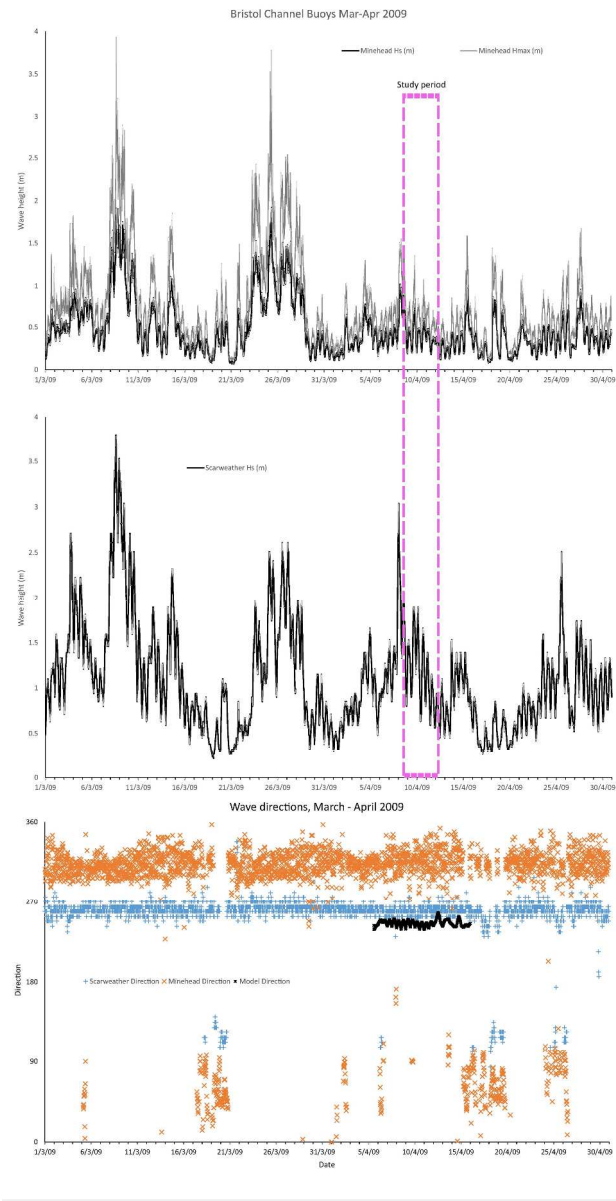
703

Table 4.

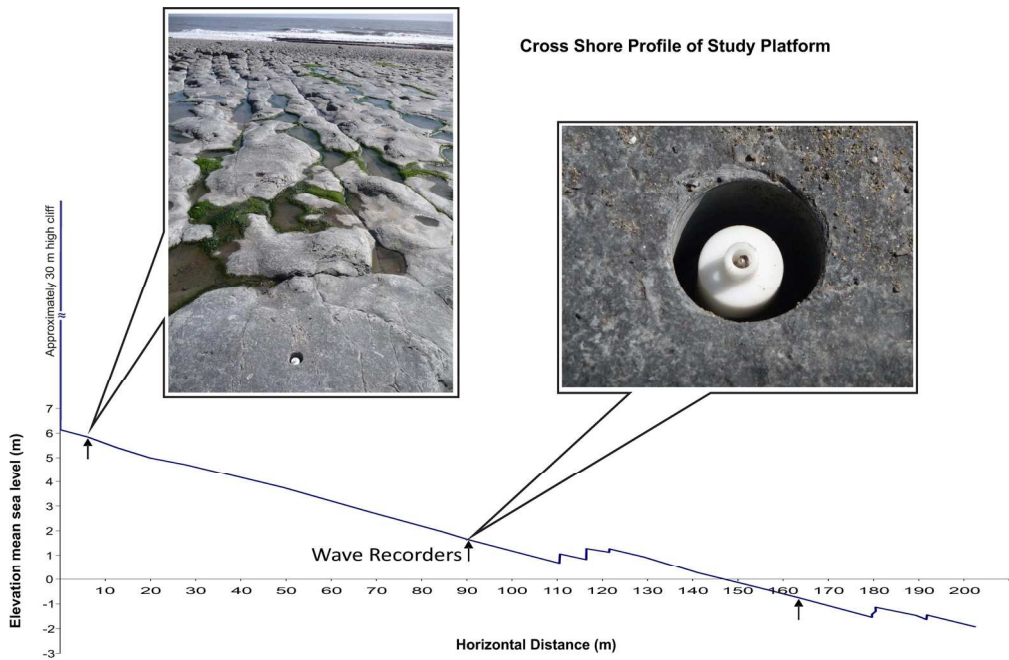
PT Location	Distance from cliff (m)	Shore Platform Elevation (m relative to MSL)	Hours of inundation over 4 days	T _{sig}	Largest H _{sig} (m)	Maximum high tide water depth (m)	Largest H _{max} at high tide	
							H _{max}	Date
Inner	6 m	5.85	26	5.0	1.43	1.55 m	2.39 m	8 April
Middle	90	1.64	52	9.0	1.35 m	5.7 m	2.41 m	9 April
Outer	163 m	-0.75	75	9.0	1.42 m	8.15 m	2.22 m	10 April



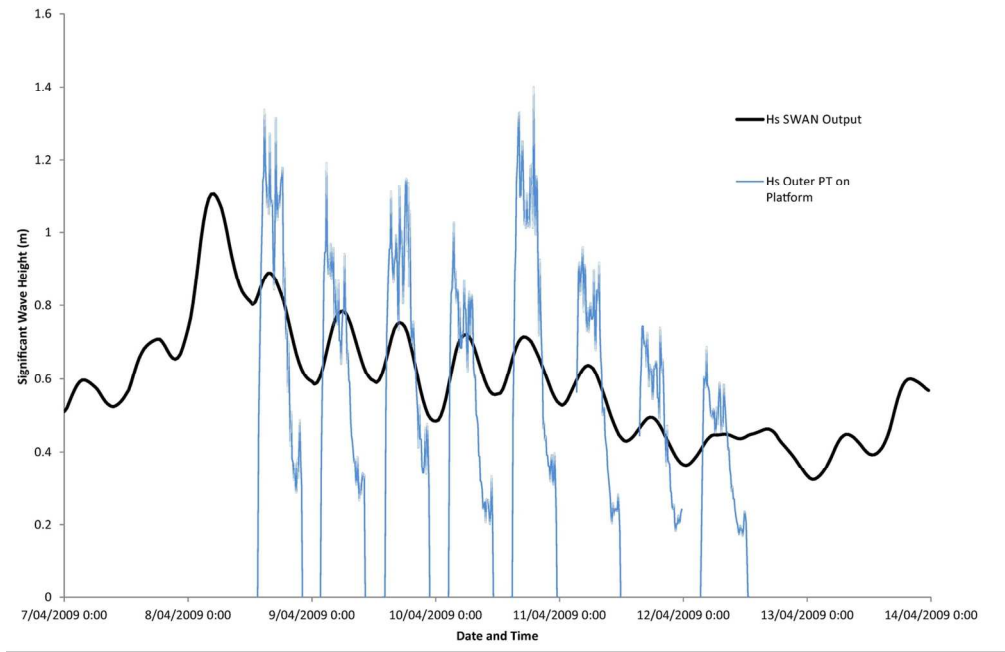
173x265mm (300 x 300 DPI)



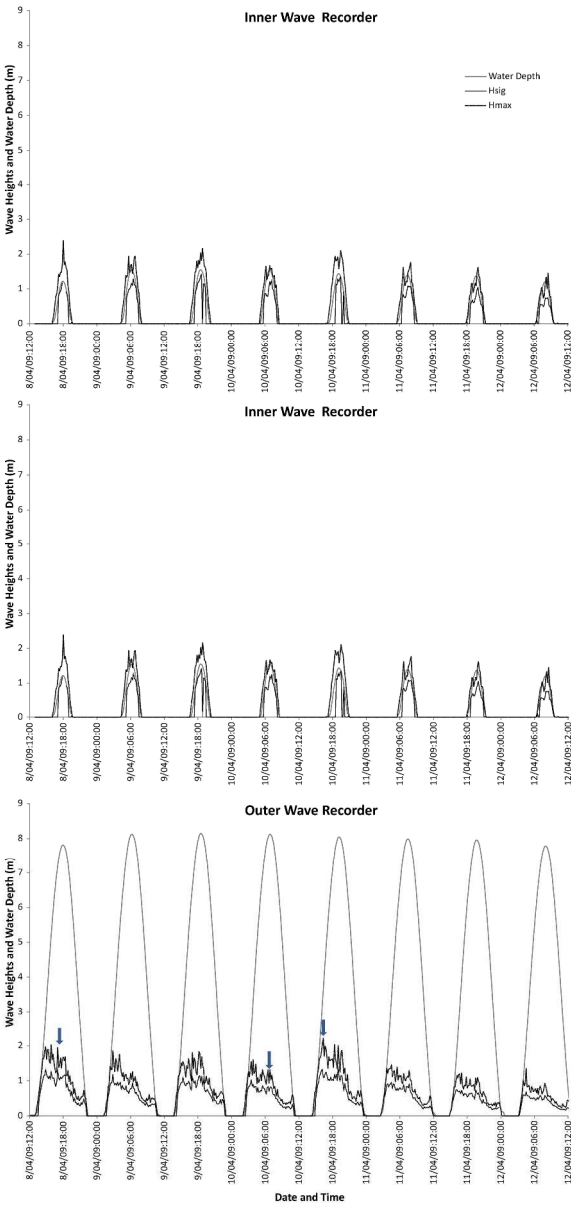
269x513mm (300 x 300 DPI)



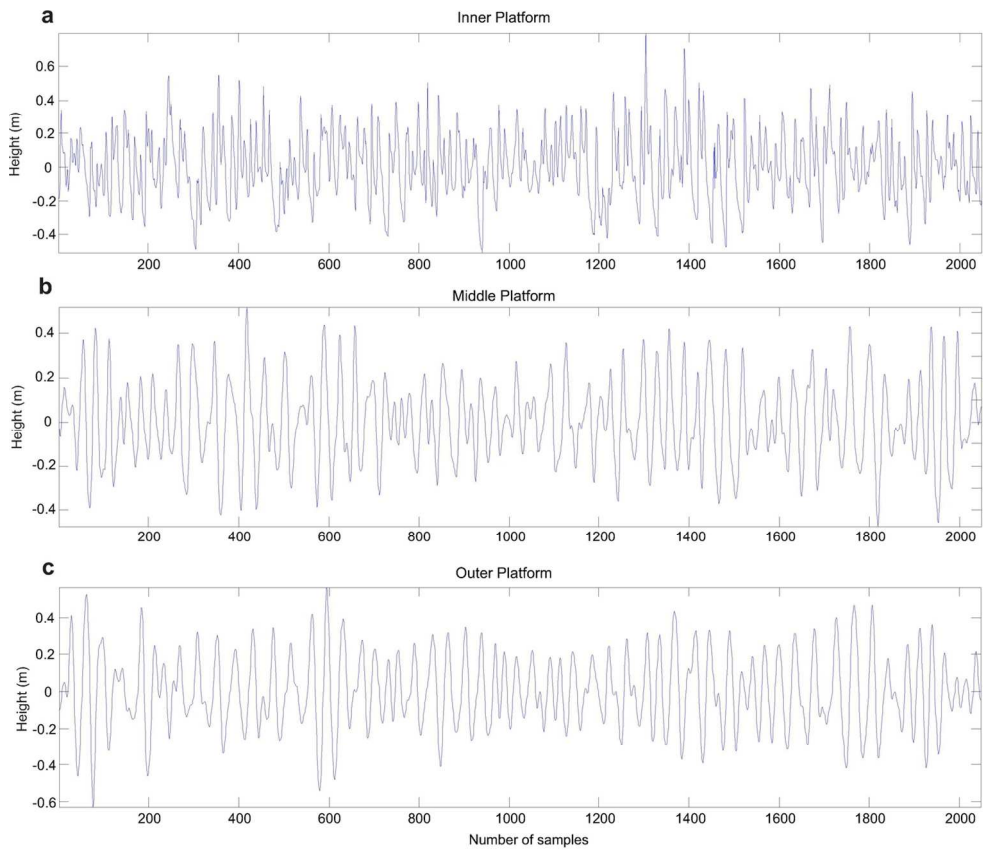
176x114mm (300 x 300 DPI)



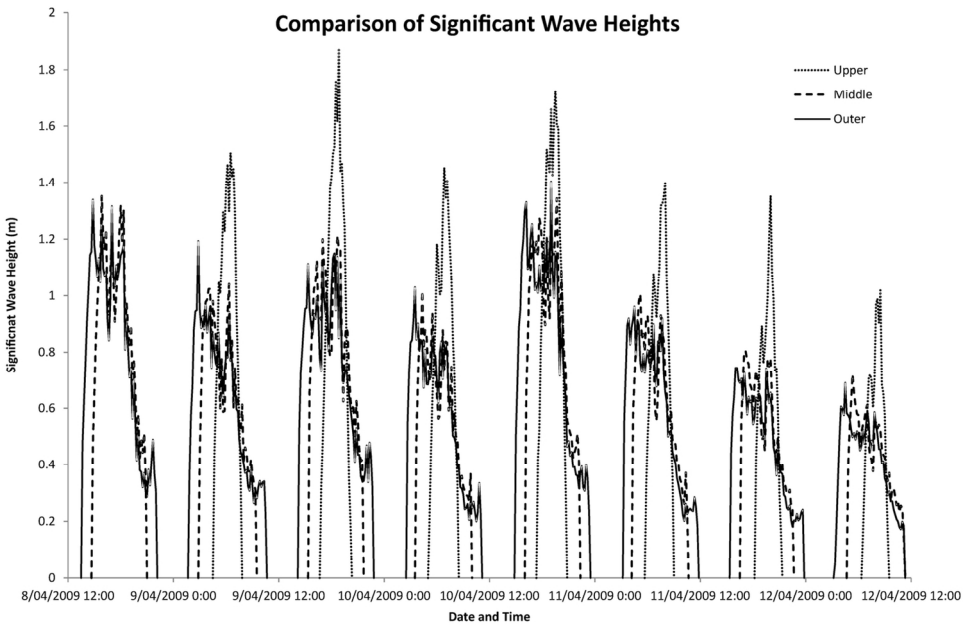
128x84mm (300 x 300 DPI)



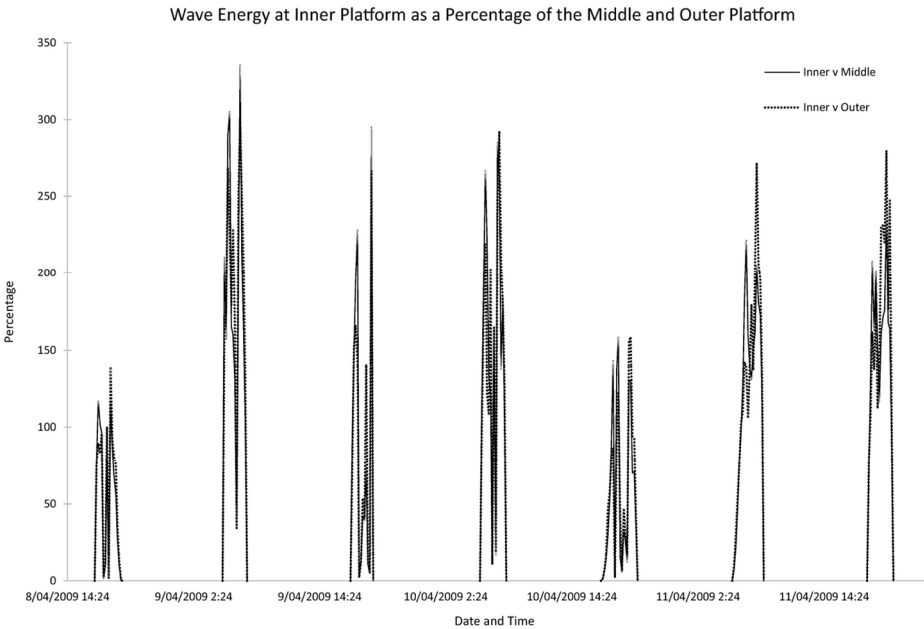
256x506mm (300 x 300 DPI)



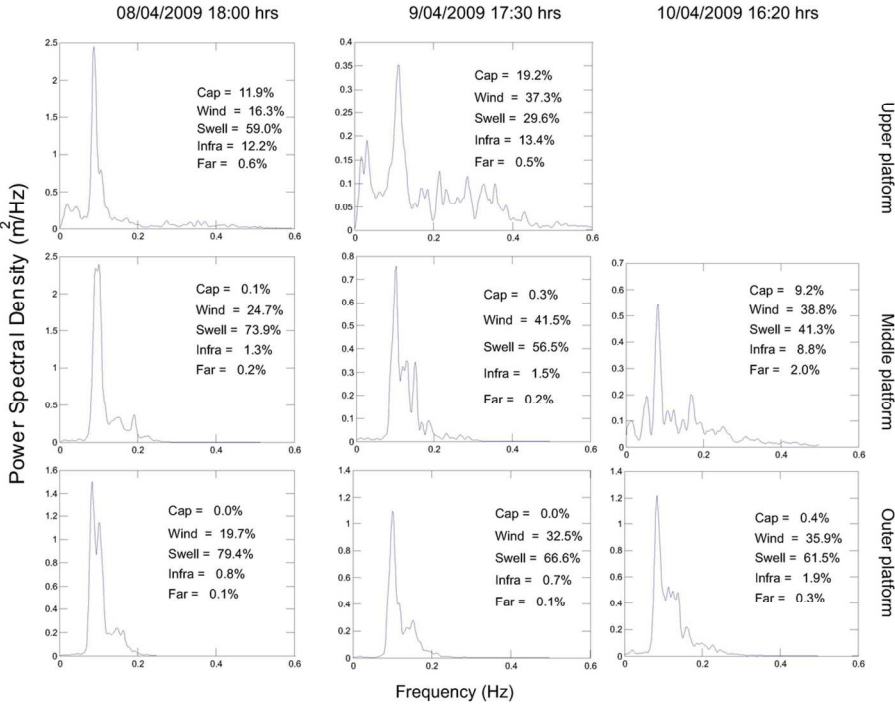
128x107mm (300 x 300 DPI)



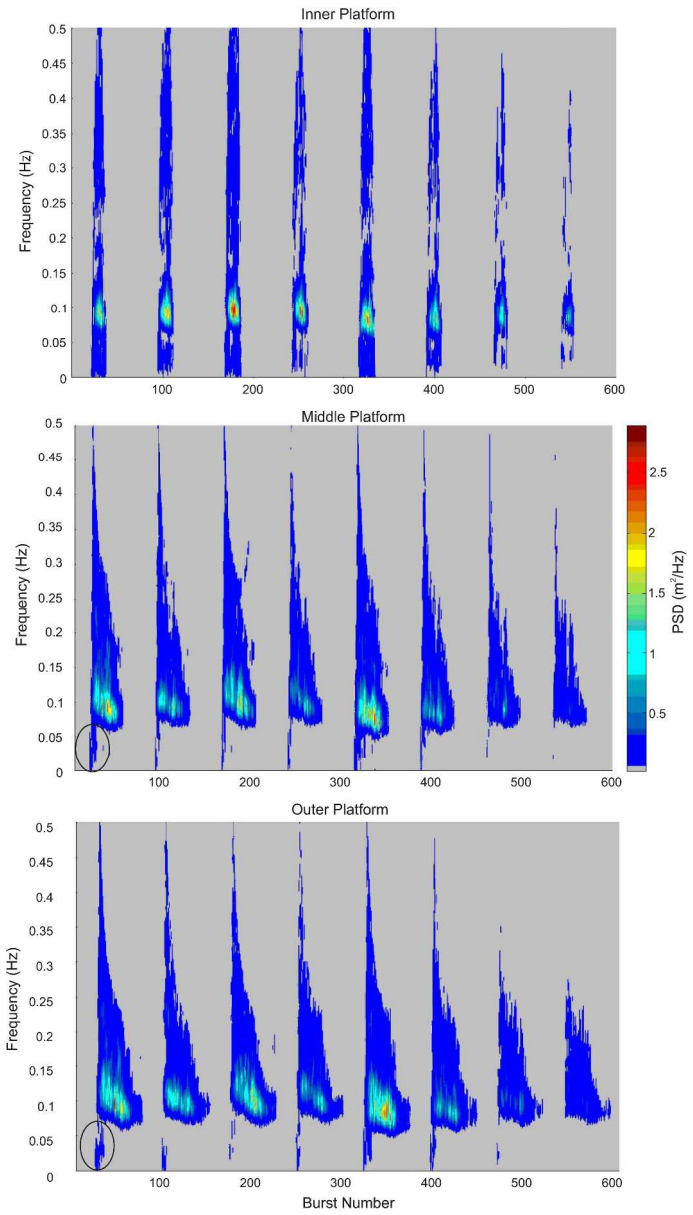
134x87mm (300 x 300 DPI)



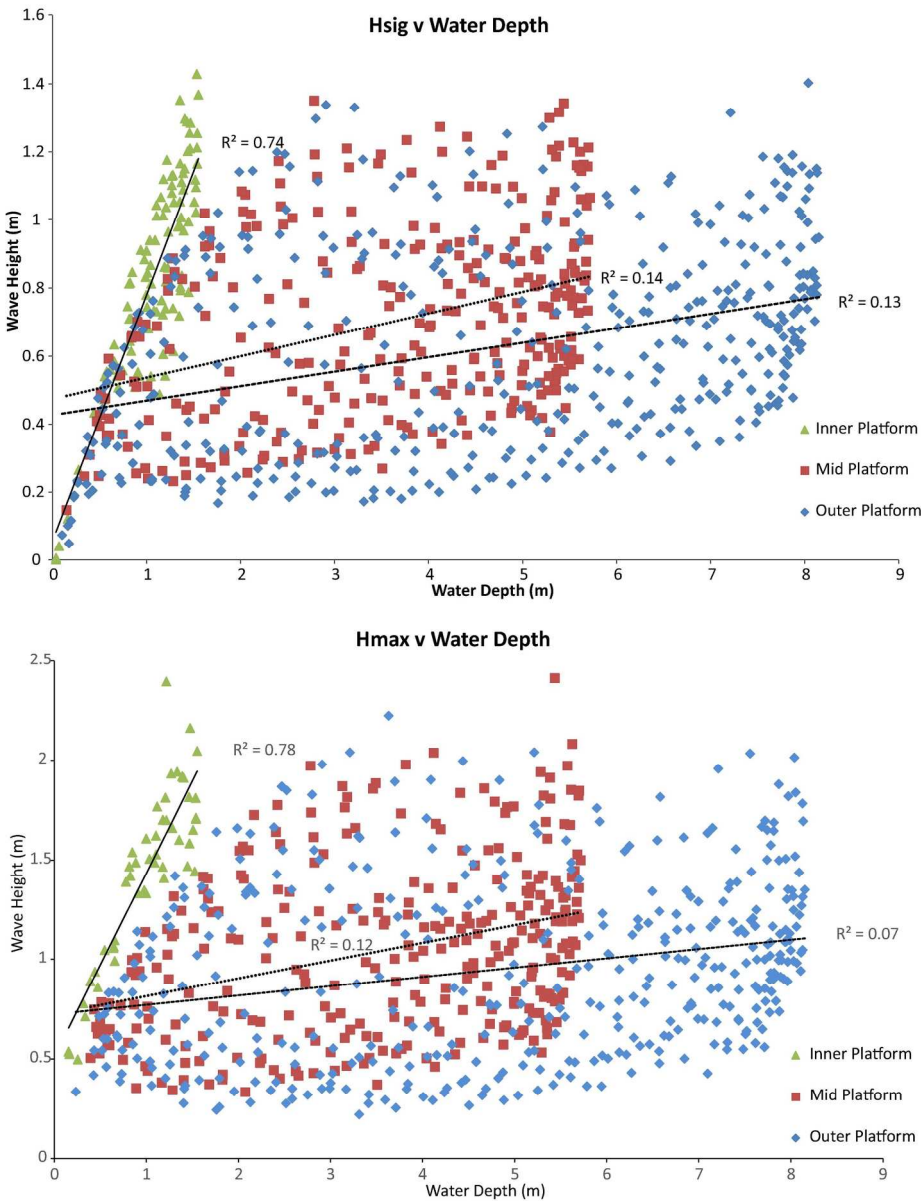
126x82mm (300 x 300 DPI)



114x79mm (300 x 300 DPI)



255x449mm (300 x 300 DPI)



168x219mm (300 x 300 DPI)

Wave Transformation across a macrotidal shore platform under low to moderate energy conditions

Wayne J. Stephenson^{*}, Larissa A. Naylor, Helen Smith, Bin Chen, Ralph P. Brayne.

We investigate how waves are transformed across a shore platform as this is a central question in rock coast geomorphology. In this macro-tidal setting, under the wave conditions measured, up to 90% of the offshore wave energy reached the landward cliff at high tide, so that the shore platform cliff is highly reflective. At high tide inner platform wave heights were generally larger than near the seaward edge and infragravity energy was less than 13% of the total energy spectra.

